Journal of
Nanoscience and Nanotechnology
Vol. 8, 1–11, 2008

Nanostructured Electrode with Titania Nanotube Arrays: Fabrication, Electrochemical Properties, and Applications for Biosensing

Peng Xiao[1, 2], Yunhuai Zhang[1, 2], Betzaida Batalla Garcia[2], Saghar Sepehri[2], Dawei Liu[2], and Guozhong Cao[2, *]

[1] *Department of Physics, Chongqing University, Chongqing, P. R. China*
[2] *Department of Materials Science and Engineering, University of Washington, Seattle, USA*

Titania nanotube (TNT) arrays were fabricated by anodic oxidation of titanium foil in various electrolytes and were calcined in dry nitrogen at various temperatures. The morphology, crystallinity, and chemical composition of TNT arrays were studied by means of X-ray diffraction (XRD) and scanning electron microscopy (SEM). Electrochemical impedance spectroscopy (EIS) was employed to investigate the electrical conductivity and capacitance of TNT arrays prior to and after calcination. The results showed that the electrical conductivities of TNT arrays calcined in nitrogen for 3 hours were improved significantly as compared to the as-grown TNT arrays or annealed in air or argon. Well defined oxidation and reduction peaks were observed during the cyclic voltammetric scans at 0.1 V/s in 10 mM $K_3[Fe(CN)_6]$ solution. For the application in biosensing, TNT electrodes co–adsorbed with horseradish peroxidase (HRP) and thionine chloride (Th) were studied for their sensitivity to hydrogen peroxide by means of cyclic voltammetric. The experiments showed that TNT arrays possessed appreciably different sensitivities to H_2O_2 due to their different conductivity. The best result was found in the TNT arrays annealed in nitrogen. Further analyses revealed that the sensitivity of TNT arrays annealed in nitrogen was increased 4–6 times compared with as-grown TNT arrays, the dynamic range on H_2O_2 is in the range of 2×10^{-5} M to 3.6×10^{-3} M at pH = 6.7 and at a potential of −600 mV (vs. Ag/AgCl).

Keywords: Titania Nanotubes Arrays, Anodic Oxidation, Calcination, Electrochemical Property, Biosensors, Hydrogen Peroxide.

RESEARCH ARTICLE

1. INTRODUCTION

The search for materials with novel microstructure and properties for applications in electrochemical sensing systems has been one of persistent focus in materials research community. Nanomaterials have a surface area three orders of magnitude greater than the micro-scale material. Hence, they offer a larger surface area for functionalization, which would greatly increase the number of binding sites for the detection of a specific chemical analyte. The discovery of carbon nanotubes[1] with their variety of interesting properties has stimulated the quest for the synthesis of nanotubular structures of other substances and chemical compounds, which possess unique combinations of physicochemical properties, and are often easier to synthesize than carbon nanotubes. Titanium is the ninth most abundant elements in the Earth's crust.[2] TiO_2, which is the most common compound of titanium, is often used for many applications ranging from dye-sensitized or organic–inorganic hybrid solar cells and photocatalysts to self-cleaning.[3–9] Also TiO_2 possesses nontoxicity, good biocompatibility and environmental safety, and has easy coordination with amine and carboxyl groups on the surface. Thus, it is widely used as matrix to immobilize proteins and enzymes as biosensor.[9–15] However, many works were focused on TiO_2 nanoparticles during the past 10 years. Bottlenecks between adjacent nanoparticles would limit the transport process and make the full coverage of self-assembled monolayer difficult. Nanotube arrays would offer both large surface area and better transport properties, thus, it is even fitter to be applied as biosensor than nanoparticles.

There are three general approaches to the synthesis of TiO_2 nanotubular structures, namely, template-assisted fabrication,[16, 17] alkaline hydrothermal synthesis,[18] and

*Author to whom correspondence should be addressed.

anodic oxidation or anodization of titanium.[19] The advantage of TiO_2 nanotubes produced by anodization is that they are readily attached onto a titanium substrate and form oriented, aligned perpendicular to the substrate, which offers much improved electron transfer pathways than non-oriented (random mixtures) structure. As a result, this oriented TiO_2 nanotubes has a great potential as electrochemical electrodes for highly sensitive (bio) sensor applications. However, an obstacle preventing TNT arrays from wide spread applications is their irreversible electrode reactions. Reduction peaks were commonly observed, but no oxidative peaks can be seen in the reverse potential scan during the cyclic voltammetric measurements due to the low electrical conductivity of titania.[20, 21] Calcination and doping are considered to be one viable approach to narrow the band gap and enhance the electrical conductivity,[22–24] however, most of the research was focused on nanocrystalline TiO_2 for applications of dye sensitized solar cells.

In this paper, TNT arrays were fabricated by anodic oxidation in different electrolyte solutions and subsequently annealed in nitrogen, air and argon. The morphology and crystal structure were characterized by means of scanning electron microscopy (SEM) and X-ray diffraction (XRD). Electrochemical impedance spectroscopy (EIS) and electrochemical analyses was employed to measure the conductivity and the electrochemical properties of TNT electrodes prior to and after calcination. The results showed that the electrical conductivity of TNT annealed in N_2 increased significantly and can be used as a new electrode material. The as-prepared TNT and TNT arrays after calcination in nitrogen co-immobilized enzyme, horseradish peroxidase (HRP), and dye, thionine chloride (Th), for the study of their sensitivities on hydrogen peroxide detection. Enzyme can be bound on TNT, this binding is mainly electrostatic and controlled by the pH, the protein charge and the solution ionic strength. It is also known that dyes are easily adsorbed from the solution to the surface of TiO_2 film, this is attributed to the chelate action between the carboxylate groups of the dye and Ti^{4+} centers of the titanium oxide surface.

RESEARCH ARTICLE

2. EXPERIMENTAL DETAILS

2.1. Reagents

Titanium foil (99.94%) of 0.5 mm in thickness, potassium fluoride (KF, 99%), hydrofluoric acid (HF, 40%), ammonium fluoride (NH_4F, 99.3%) and ethylene glycol (100%) were purchased from VWR, and horseradish peroxidase (HRP, 2.5 mg/ml), thionine chloride (Th, 100%) were from Sigma. Chemicals were of reagent grade and were used as received. All the solutions were prepared with DI water ($>16\ M\Omega \cdot cm$).

2.2. Fabrication of TNT Arrays

TNT arrays were fabricated by anodization of Ti foil in a two-electrode electrochemical cell with a platinum foil as a cathode at a constant potential at room temperature, following the recipe reported in literatures.[25–27] The Ti substrate was polished using SiC powder (grit 600), followed by diamond paste (grade 1, particle size $< 2\ \mu m$), and then chemically etched in 30% HCl aqueous solution at approximately 80 °C for about 20 min. After rinsing thoroughly with DI water, the clean titanium foils were anodized in three different types of electrolytes for 1 hour to form TNT arrays on Ti substrates. The composition of three electrolyte solutions and the voltage used for anodization were summarized in Table I. The resultant TNT arrays are hereinafter designated as: TNT(HF), grown in 0.1 M HF electrolyte, TNT(KF), in the mixture electrolyte of 1.0 M $NaHSO_4$ and 0.1 M KF, and TNT(EG), in the ethylene glycol (EG) containing 0.25% NH_4F.

2.3. Calcination of TNT Arrays in Nitrogen

For investigating the annealing effect to TNT arrays, the as-grown TNT(KF) arrays fabricated in the mixture electrolyte of 1.0 M $NaHSO_4$ and 0.1 M KF at 20 V were calcined at temperatures ranging from 300 to 650 °C in tube furnace, under a flow of dry N_2, with a heating rate of 4 °C/min and dwelled time between 1 and 6 hours. In order to compare with the effects of calcination in nitrogen, the as-grown TNT(KF) was also calcined in air and argon at the same temperatures respectively. The resultant TNT(KF) arrays are hereinafter designated as: TNT/N_2, for nitrogen-calcination, TNT/Ar, for argon-calcination and TNT/air, for air-calcination.

2.4. Preparation of Modified Electrodes

The three as-grown TNT arrays, TNT(HF), TNT(KF), TNT(EG), and one TNT(KF) arrays after annealing in nitrogen (TNT/N_2) were first rinsed by DI water thoroughly, sealed with epoxy resin leaving an open area of $0.7 \times 0.7\ mm^2$, then immersed in 1 ml 5 mM PB solution

Table I. Summary of electrolyte compositions and anodization voltages as well as the diameters, length, and specific surface area of the resultant TNT arrays.

Samples	Electrolyte composition	Voltage (V)	Diameter (nm)	Length (μm)	Surface area (mm^2/mm^2)
TNT(HF)	0.1 M HF	20	100	0.5	8
TNT(KF)	0.1 M KF + 1.0 M $NaHSO_4$	20	110	1.2	17
TNT(EG)	0.25% NH_4F + Ethylene glycol	60	80	12	692

at pH 7.0 containing 15 μM thionine chloride and 200 μL HRP for 2 days to produce the Th/HRP modified electrodes. For the measurements of HRP and Th loading, UV-Vis absorption spectra of the mixed HRP/Th solution before and after immersion were measured. The absorption peak intensities at 415 nm for HRP and at 603 nm for Th were used to estimate the amount of HRP and Th adsorbed on the TNT surface. The resultant electrodes were stored in 5 mM PB of pH 7.0 at 4 °C.

2.5. Characterization

For characterizing TiO_2 nanotubes morphology, diameter, and length, a scanning electron microscope (SEM, Philips, JEOL JSM7000) was employed with an accelerating voltage 10 kV, and the elemental composition analysis of nanotubes were performed by means of energy dispersive X-ray spectroscopy (EDX). X-ray diffraction (XRD) was performed on a Philips 1820 X-ray diffractometer with $Cu_{K\alpha}$ radiation ($\lambda = 1.5418$ Å). For all the XRD analyses, TiO_2 nanotubes were scratched from the substrates and placed in standard plastic sample holders.

2.6. Electrochemical Measurements

Cyclic voltammetric was performed with a CHI605IC electrochemical station, and electrochemical impedance spectroscopy (EIS) was carried out in a Salon 1260 impedance/gain-phase analyzer. A Pt foil and Ag/AgCl electrode were used as counter electrode and reference electrode respectively. Electrochemical software Z-plot was employed for impedance data acquisition. The amplitude of the modulation potential for EIS measurement was 10 mV, the range of the frequency was from 400 kHz to 0.05 Hz. All solutions were deaerated with ultrapure nitrogen before measurements, and nitrogen was passed over the top of the solution during the experiments. All measurements were conducted at room temperature (about 20 °C).

3. RESULTS AND DISCUSSION

3.1. Morphology and Crystallization Characterization

Figure 1 is the SEM images of TNT arrays prepared in different electrolytes for 1 hour. Uniform TNT arrays have been grown by acidic anodization in all three different electrolyte solutions, and all the TNT arrays adhered very well to the underneath Ti substrates. However, the grown TNT arrays vary significantly in nanotube size and length depending on the applied DC voltage, anodization time, and the type of electrolyte solutions. The average pore diameters of TiO_2 nanotubes as estimated from the SEM images are 100 nm (TNT(HF)), 110 nm (TNT(KF)), and 80 nm (TNT(EG)), and the lengths of the nanotubes are 500 nm (TNT(HF)), 1.2 μm (TNT(KF)), and

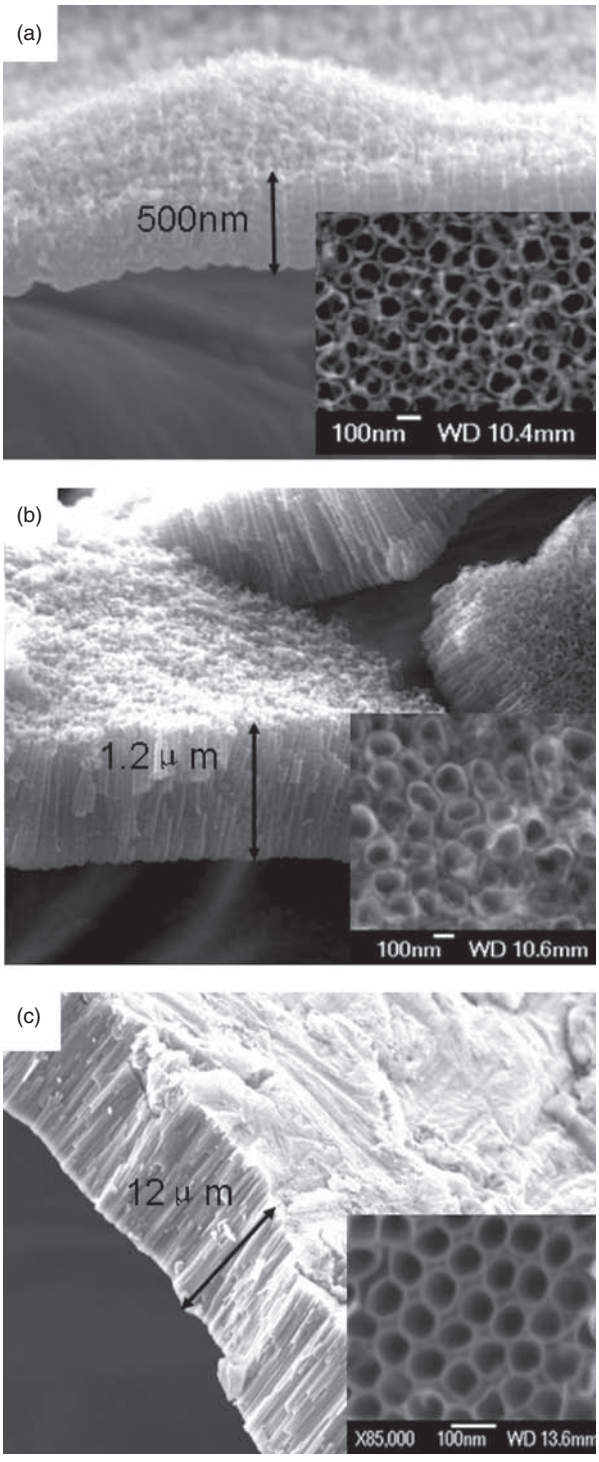

Fig. 1. SEM images of TiO_2 nanotubes prepared in (a) 0.1 M HF acid solution at 20 V (b) 1.0 M $NaHSO_4$ containing 0.1 M KF at 20 V (c) ethylene glycol containing 0.25% NH_4F at 60 V for 1 hour.

12 μm (TNT(EG)), respectively. The specific surface area are estimated to be 8 (cm^2/cm^2) (TNT(HF)), 17 (cm^2/cm^2) (TNT(KF)) and 690 (cm^2/cm^2) (TNT(EG)), respectively. The length of nanotube arrays are affected by both the pH value of electrolyte solutions and the water content. In

RESEARCH ARTICLE

hydrogen fluoride aqueous electrolyte (pH = 1.2), it is not possible for nanotube length to be greater than 500 nm, which corroborates with the results reported in literature.[28] In a KF electrolyte by adjusting the pH to 4.0 through the addition of sodium hydrogen sulfate and sodium hydroxide, the length of TiO_2 nanotubes could grow to 1.2 μm for one hour anodization.[25] While in the organic electrolyte, the reduction of water content reduces the solubility of the TiO_2 nanotubes and thus promotes the growth of longer nanotubes.[26] The spectra curves of the EDX analyses for the TNT arrays indicated that other than Ti, and O, there exist traces F and C in these arrays.

Figure 2 shows the top and side morphology SEM images of TNT(KF) arrays with calcinations (a) and after calcination in N_2 at 300 °C for 3 hrs (b), 500 °C for 3 hrs (c) and for 6 hrs (d). The average diameter and wall thickness of TNT were estimated from the SEM images and averaged over a large area. Prior to calcination, the TNT has an inner diameter of ~100 nm and wall thickness ~9 nm, the length of the tube is 1.2 μm. After calcined at 300 °C and 500 °C for 3 hrs, the inner diameters decreased to 90 nm and 78 nm, while the wall thickness increased to 14 nm and 20 nm, and the length decreased to 1.1 μm and 1.0 μm respectively. A prolonged annealing at 500 °C in N_2 for 6 hrs resulted in the collapse of TNT arrays. The wall thickness increased to 30 nm with most of the nanotube wall stuck together. These results indicate sintering of TNT arrays occurred during calcinations at temperatures above 300 °C. As expected, the increase of wall thickness was accompanied with a decrease in the length of TNT according to SEM cross-section images. Such a change of morphology is thermodynamically favorable, as it results in a reduction of specific surface area and thus the total surface energy. Nanostructures or nanomaterials, possessing large specific surface area and thus surface energy, are thermodynamically metastable,[29] and would change their morphologies under favorable conditions. Since sintering is an activated process involving mass transfer,[30] a higher annealing temperature or a prolonged annealing time favors more sintering and tends to destroy nanostructures completely. It should be noted that similar morphology change was observed when TNT

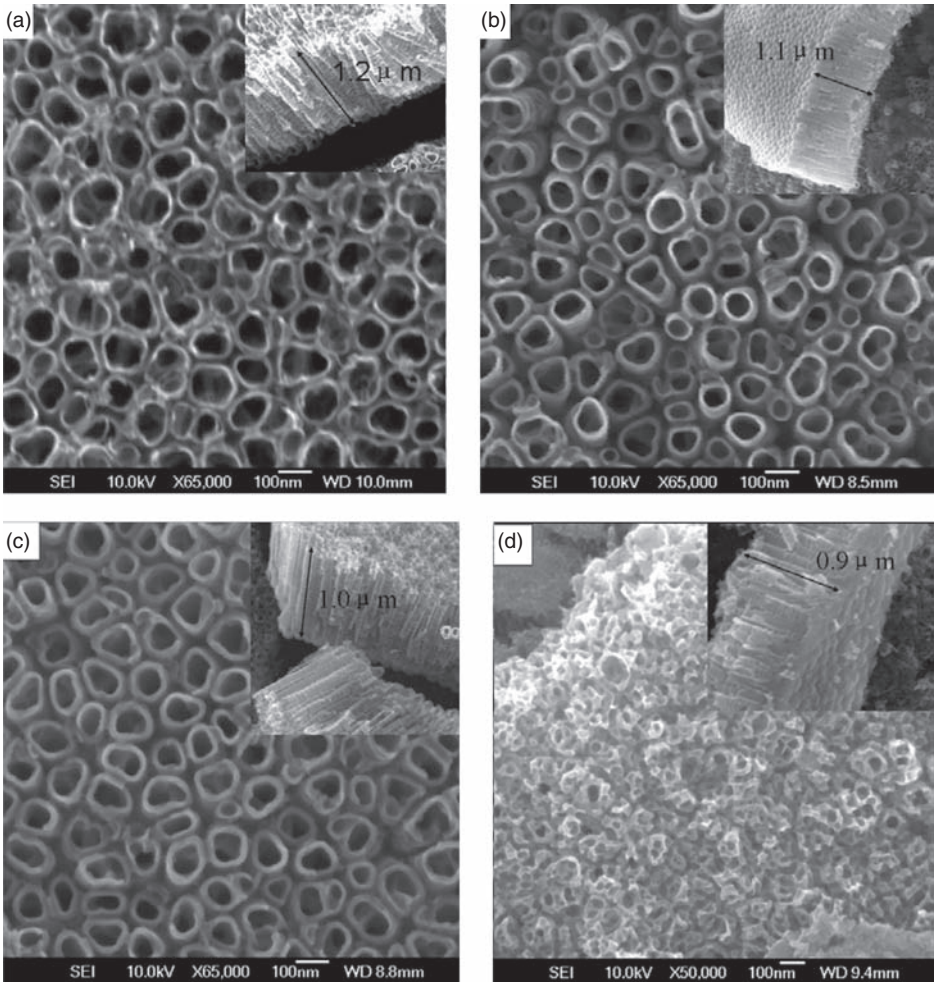

Fig. 2. SEM images of TiO_2 nanotubes fabricated in the mixture electrolyte of 1.0 M $NaHSO_4$ and 0.1 M KF at 20 V (a) before calcination (b) calcined in N_2 at 300 °C for 3 hours (c) calcined in N_2 at 500 °C for 3 hours (d) calcined in N_2 at 500 °C for 6 hours.

RESEARCH ARTICLE

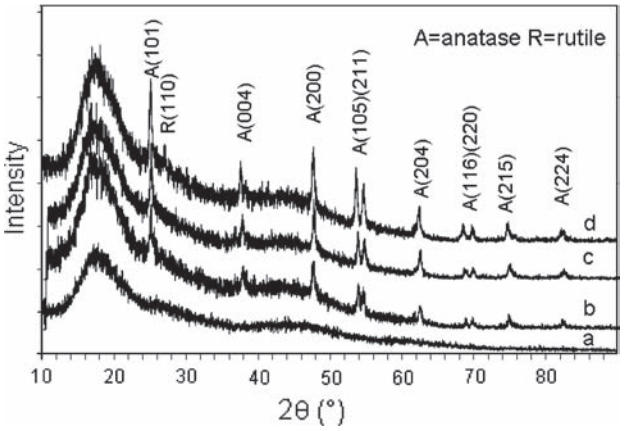

Fig. 3. XRD pattern of TNT arrays before calcination (a) and after calcined in N_2 at (b) 300 °C (c) 500 °C and (d) 650 °C for 3 hours.

arrays were calcined in argon under otherwise the same conditions. However, when calcined in air, TNT morphology are more stable and will only be destroyed when fired at 500 °C for over 9 hrs. EDX results showed that there only existed C, Ti, and O, F trace was disappeared after calcination.

Figure 3 are the XRD patterns of TNT arrays before calcination and after calcined in N_2 for 3 hrs at different temperatures. Before calcination, all the as-grown TNT arrays are amorphous as determined by XRD, crystallization in amorphous TNT arrays occurred at a temperature as low as 300 °C. The XRD peaks of anatase phase are unambiguously visible, indicating the phase transition from amorphous to anatase crystal. Heating at higher temperatures such as 650 °C, resulted in the formation of rutile phase. The phase formation and transition temperatures observed in this work are in a good agreement with the literature data.[31, 32] Such phase transition would promote sintering process. In spite of some trivial differences when annealed at higher temperatures, the TNT arrays calcinated at 500 °C for 3 hrs possess similar morphology and XRD patterns regardless the annealing gas atmospheres. It is noted that the broad peak at ~18° reflects the amorphous nature of the sample holders and the fact that a small quantity of samples was available for the measurements.

3.2. EIS Measurement

Electrochemical impedance spectroscopy (EIS), as a powerful technique widely used to study porous electrodes[33–35] was employed to investigate the electrical conductivity of the as-grown TNT arrays fabricated in different electrolytes and TNT arrays calcinated at 500 °C for 3 hours in different gases. All measured at the electrode potential 0.1 V in 0.1 M Na_2SO_4 at frequencies ranging from 0.05 Hz to 40 kHz. An equivalent circuit $R_1(R_2C_2)(R_3\text{CPE})$, shown in Figure 4, was often used to model the impedance data of porous material film according to the literature.[34] In this equivalent circuit, R_1 represents the uncompensated

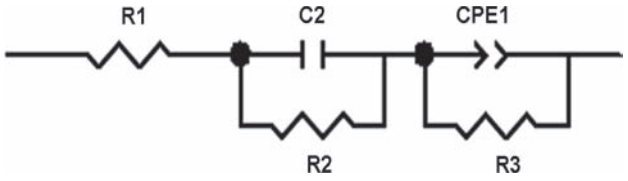

Fig. 4. Equivalent circuit.

solution resistance; the parallel combination R_2C_2 is associated with the resistance and capacitance of the TNT electrodes. The parallel combination of the charge transfer resistance (R_3) and the constant phase element (CPE) leads to a depressed semicircle in the corresponding Nyquist impedance plot.[35] All the fitting data was deduced directly using the electrochemical software Z-plot. The constant phase element (CPE) is defined by CPE-T and CPE-P. If CPE-P equals 1 approximately, then the CPE is identical to a capacitor, C_{dl}.[34]

Figure 5 presents Nyquist plot of three as-grown TNT electordes fabricated in different electrolytes, where Z' and Z'' are real and imaginary components of the impedance, respectively. The fitting curves are shown in figure as solid lines together with the experimental data denoted as symbols. The parameters determined by the fitting of the experimental EIS data in the solution are summarized in Table II.

The electrical resistance R_2 of as-grown TNT arrays increases in the following order: TNT(HF) (2.78×10^5 Ω) < TNT(KF) (9.19×10^5 Ω) < TNT(EG) (14.33×10^5 Ω), and the capacitance C_2 changes as: TNT(HF) (3.77 μF) < TNT(KF) (6.65 μF) < TNT(EG) (9.89 μF). The above results can be qualitatively explained by the lengths of the TiO_2 nanotubes and thus the surface area.

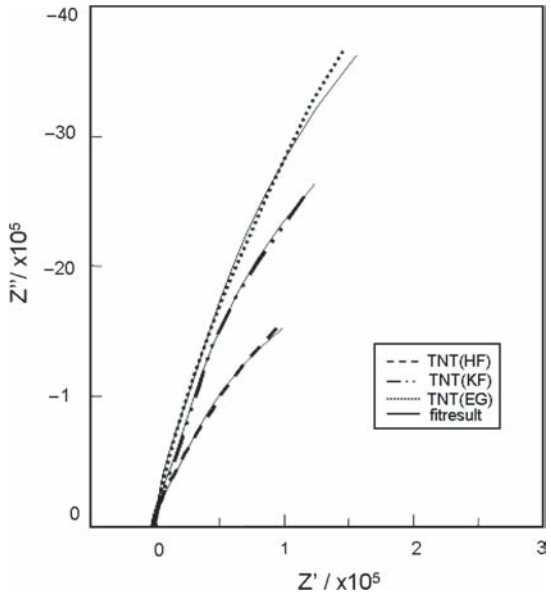

Fig. 5. Nyquist plots of TNT(HF) (dash line), TNT(KF) (dash and dot line) and TNT(EG) (dot line) in 0.1 M Na_2SO_4 solution. The solid line is the fitting curve.

RESEARCH ARTICLE

Table II. Impedance components for as-grown TNT arrays determined by fitting EIS experimental data using the equivalent circuit shown in Figure 4.

TNT arrays	$R_1(\Omega)$	$R_2(\times 10^5\ \Omega)$	$C_2(\mu F)$	$R_3(\times 10^5\ \Omega)$	CPE-P	CPE-T (μF)
TNT(HF)	227	2.78	3.77	5.08	0.832	6.45
TNT(KF)	222	9.19	6.65	5.51	0.856	8.45
TNT(EG)	214	14.33	9.89	7.54	0.870	5.81

TNT(HF) has the shortest length of 500 nm with a diameter of 100 nm, while the TNT(KF) has a length of 1.2 μm and a diameter of 110 nm. Considering the electrical resistance is directly proportional to the length and inversely proportional to the cross section area, it is reasonable to have such a trend of increased resistance from TNT(HF) to TNT(KF) to (TNT(GE). TNT(EG) has a length of 12 μm, almost 30 times of that of TNT(HF) and, thus, possesses almost 7 times the electrical resistance. It should be noted that the resistance of the TNT electrodes is not the resistance between the two ends of the nanotubes, instead it is the resistance between the electrolyte solution and the bottom charge connecting electrode Ti substrate. Therefore, it is difficult, if not impossible, to establish a simple direct and quantitative relationship between the size and the electrical resistance. The capacitance is proportional to the surface area; however, the difference in surface area is obviously not the only factor to affect the capacitance of TNT electrodes in this study. Surface chemistry may play a significant role here.

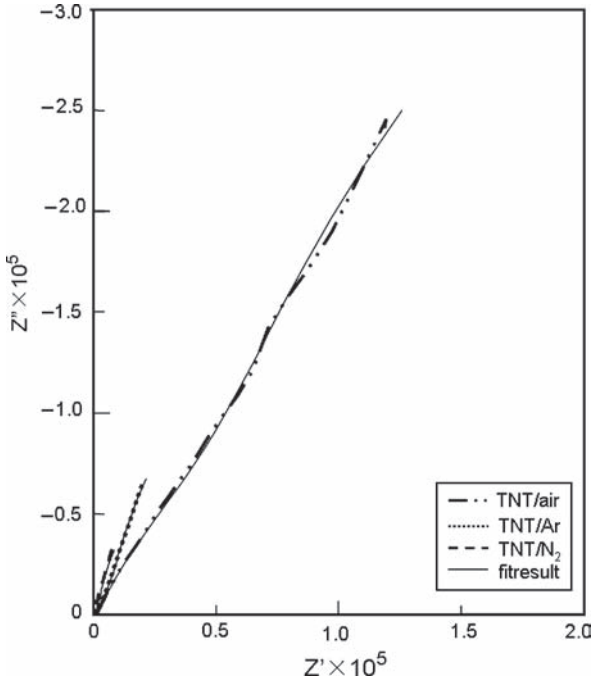

Fig. 6. EIS spectra of TNT/air (dash dot line), TNT/Ar (dot line) and TNT/N_2 (dash line) electrodes calcinated at 500 °C for 3 hours. The solid line is the fitting curve.

Table III. Impedance components for TNT electrodes calcinated at 500 °C for 3 hours in different gas and determined by fitting EIS experimental data using the equivalent circuit shown in Figure 4.

Electrodes	$R_1(\Omega)$	$R_2(\times 10^5\ \Omega)$	$C_2(\mu F)$	$R_3(\times 10^5\ \Omega)$	CPE-P	CPE-T (μF)
TNT/air	149	6.92	16.56	3.71	0.746	15.75
TNT/Ar	175	3.95	23.8	1.15	0.739	39.2
TNT/N_2	130	1.94	48.9	0.36	0.734	98.6

EIS spectra of TNT arrays calcined in different gases, TNT/air (dash dot line), TNT/Ar (dot line) and TNT/N_2 (dash line) electrodes were presented in Figure 6. The parameters determined by the fitting of the experimental EIS data in the solution are summarized in Table III. The resistance, R_2, of the TNT electrodes changed in the following order: $6.92 \times 10^5\ \Omega$ (TNT/air) > $3.95 \times 10^5\ \Omega$ (TNT/Ar) > $1.94 \times 10^5\ \Omega$ (TNT/N_2). The charge transfer resistance, R_3, decreased in the following order: $3.71 \times 10^5\ \Omega$ (TNT/air) > $1.15 \times 10^5\ \Omega$ (TNT/Ar) > $0.36 \times 10^5\ \Omega$ (TNT/N_2), the charge transfer resistance R_3 of TNT/N_2 is 14 times lower than amorphous TNT arrays and a factor of 5–10 enhancements than TNT/air and TNT/Ar, these results showed that the TNT arrays calcined in N_2 possesses higher electrical conductivity than as-grown TNT and TNT arrays calcined in air or argon.

3.3. Electrochemical Properties

The electrochemical properties of TNT electrodes before and after annealed were investigated by means of cyclic voltammetry (CV) with 10 mM $K_3[Fe(CN)_6]$ as an electrolyte in a potential range of −1.0–1.6 V versus Ag/AgCl at a sweep rate of 0.1 V/s. Figure 7 are the CV results of three as-grown TNT electrodes. For the TNT before annealed, a well-defined reduction peak appears at −0.6 V for the TNT(HF) and TNT(KF) electrodes, while no reduction peak is observed for the TNT(EG) electrode in the same potential range. No oxidative peaks are seen in the reverse scans for all three electrodes, which indicated a non-reversible electrochemical reaction of $K_3[Fe(CN)_6]$ on the electrodes. This result is due to the low electrical conductance and consistent with the electrochemical and spectroelectrochemical studies of nanoporous TiO_2 films by Topoglidis et al.[20, 36] Figures 8(A) and (B) are the CV results of TNT electrodes calcined at 500 °C for 3 hours in different gases. TNT/air and TNT/Ar electrodes have oxidation peaks at 0.974 V and 1.209 V and reduction peaks at −0.343 V and −0.302 V, respectively. Their reduction-oxidation peak separation was approximately 1.317 V and 1.511 V, respectively. The large peak separation is attributed to the low electrical conductivity of the TNT electrodes. This observation agrees well with the EIS data described in the previous section. It should be noted that as grown amorphous TNT electrode possessed only a reduction peak, but no oxidation peak appeared at

RESEARCH ARTICLE

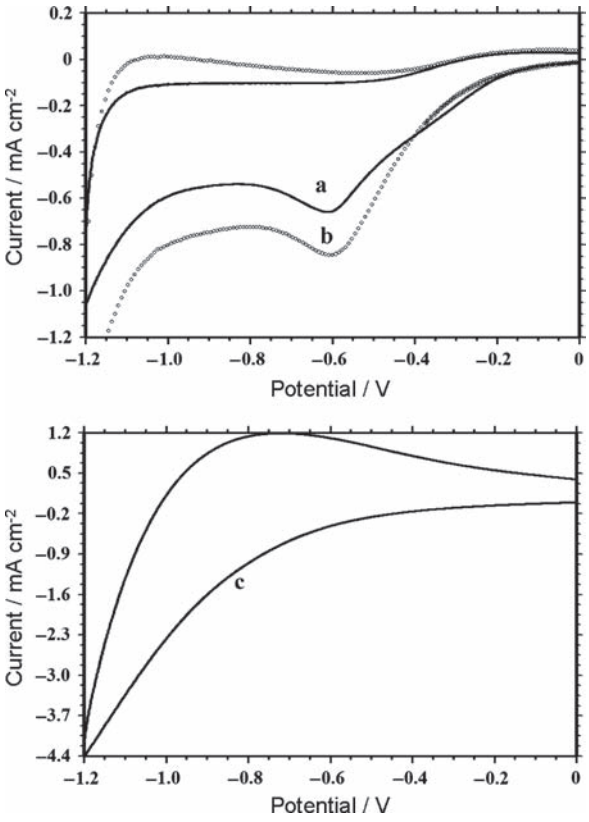

Fig. 7. Cyclic voltammetry of 10 mM $K_3[Fe(CN)_6]$ with (a) TNT(HF) (b) TNT(KF) and (c) TNT(EG) electrodes.

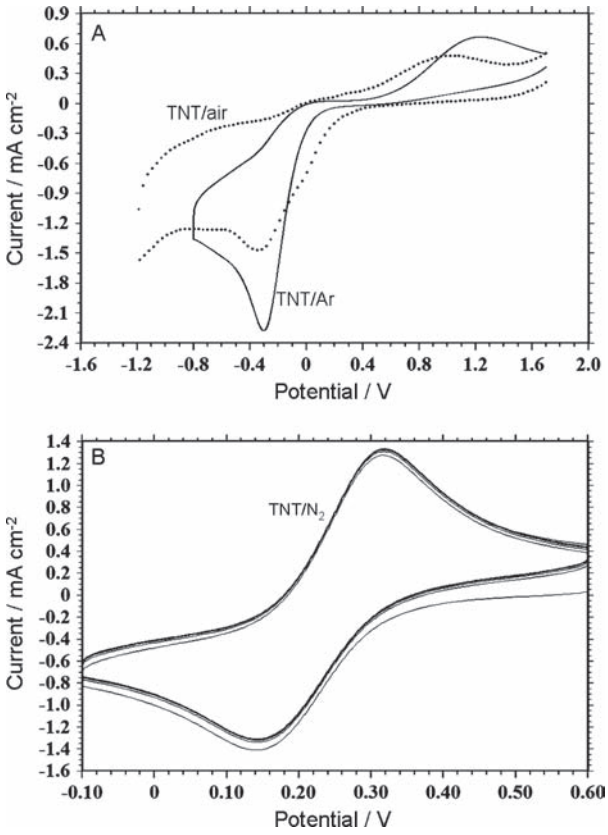

Fig. 8. Cyclic voltammetry of 10 mM $K_3[Fe(CN)_6]$ with (A) TNT/air (dot line) and TNT/Ar (solid line) electrodes (B) TNT/N_2 electrode of 20 cycles calcined at 500 °C for 3 hours.

the reversed scan, which was ascribed to the further lower electrical conductivity. Figure 8(B) shows 20 cycles of CV results of TNT/N_2 electrode. TNT/N_2 electrode possesses a pair of well-defined oxidation/reduction peaks centered at 0.15 V and 0.31 V and the peak separation was 0.16 V. The peak current density equals to 1.35 mA cm^{-2}, which is larger than the current of TNT/air and TNT/Ar. Except the first cycle, there is no appreciable change in the peak positions of both oxidation and reduction reactions, nor in the peak current density, which showed that the electrode reaction was very stable. Figure 9(A) is the CV results of 10 mM $K_3[Fe(CN)_6]$ with TNT/N_2 electrode at different scan rates, and the two curves of plot B is the anodic peak current and cathodic peak current change with the scan rate. The linear fitting results of the two curves are as follows,

$$j_{pa} = 1.12 + 49.69v^{1/2} \quad (1)$$

$$j_{pc} = 1.69 + 39.93v^{1/2} \quad (2)$$

Where j_{pa} and j_{pc} are the anodic current density and cathodic current density; v refers to the scan rate. The correlation coefficients are 0.999 and 0.998, respectively. The current density are proportional to the square root of scan rate, which suggested a quasi-reversible electrochemical reaction of $K_3[Fe(CN)_6]$ for the TNT/N_2 electrodes. The electron transfer constant is $k^0 = 1.87 \times 10^{-3}$ cm/s. The reduction and oxidation peaks can be ascribed respectively to the reduction and oxidation reactions of electroactive probe molecule, $K_3[Fe(CN)_6]$ on the TNT electrode surface. For less conductive electrode, it is difficult for electroactive probe molecules to lose electrons on the electrode surface, so the oxidation current density is lower than the reduction current density. Ghicov and co-authors also observed oxidation/reduction peaks for anatase π-TiO_2 tube electrode,[37] but these peaks are ascribed to the intercalation and release of H^+ on the π-TiO_2 layer surface, which presented the oxidation of Ti^{3+} and reduction of Ti^{4+}. It is worthy further notice that their peak separation was of ~0.3 V for annealed TiO_2 tubes, which is bigger than that in TNT/N_2 electrode (~0.16 V).

There are two possible effects on TNT arrays when annealed in nitrogen. One is nitrogen doping in TNT arrays through substitution of oxygen in anatase with nitrogen as reported in literature.[24] Considering the experimental conditions used in the current study, the annealing temperature below 500 °C in dry nitrogen without any catalyst, nitrogen doping is very unlikely as the nitrogen molecules with triple chemical bonds are very stable. Another possible effect is the partial reduction of tetravalent titanium cations. Annealing under a reductive

RESEARCH ARTICLE

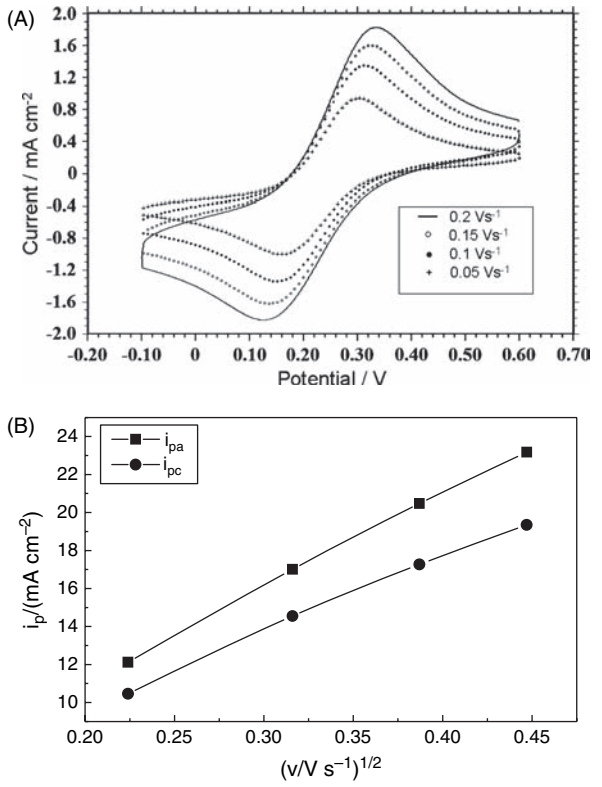

Fig. 9. (A) Cyclic voltammetry of 10 mM $K_3[Fe(CN)_6]$ with TNT/N_2 electrode at different scan rates (B) Anodic peak current and cathodic peak current change with the scan rate.

environment, such as in nitrogen, is likely to result in reduction of part of Ti^{4+} cations to lower valence state. This partial reduction of tetravalent titanium cations would be accompanied with the formation of oxygen vacancies. That in turn would change the electrical properties of the material. Change of electrical properties of oxides through thermal annealing under various gases is well established in literature.[38] Such impact would become more significant in nanostructured materials due to the huge surface to volume ratio.

3.4. TNT Arrays as Biosensor Application

3.4.1. Co-Adsorption of HRP and Th on TNT Arrays

Immobilization of both HRP and Th on the TNT arrays reached saturation after immersing TNT arrays in the mixture solutions of HRP and Th for 2 days. Figure 10 shows the absorbance spectra of the as-prepared mixture solution (dash line) and remaining solution (solid line) with HRP and Th adsorbed by TNT(EG) electrode for 2 days. Absorption peaks of HRP at 415 nm and Th at 603 nm are appreciably reduced, indicating both HRP and Th were removed from the solution and co-immobilized on the TNT(EG) electrode. The amounts of HRP and Th adsorbed were estimated from the change of peak intensities. The same measurements of absorbance spectra were carried

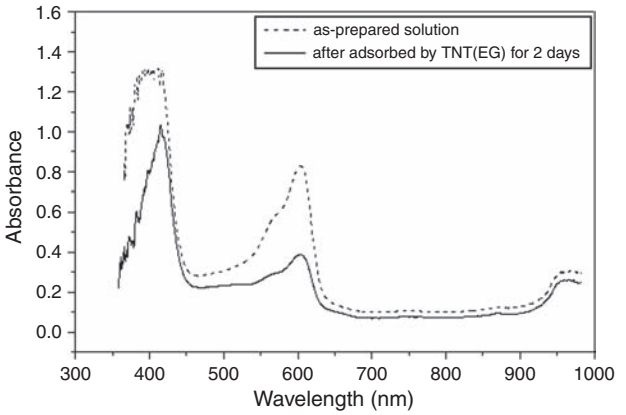

Fig. 10. Absorbance of HRP and Th in as-prepared mixture solution of 15 μM Th and 200 μL HRP in 1 ml 5 mM PB (dash line) and remains solution (solid line) after adsorbed by TNT(EG) electrode for 2 days.

out on TNT(HF), TNT(KF) and TNT/N_2 electrodes and revealed the similar results of co-adsorption of HRP and Th, though with varied amounts being adsorbed. Table IV summarized the amount of HRP and Th adsorbed on three different TNT samples. These results revealed that both HRP and Th can be effectively immobilized on TNT arrays by a co-adsorption procedure. However, the amounts of Th adsorbed on TNT electrodes increased significantly from 1.1 $\mu g/mm^2$ on TNT(HF), to 2.6 $\mu g/mm^2$ on TNT/N_2, to 2.7 $\mu g/mm^2$ on TNT(KF), to 3.8 $\mu g/mm^2$ on TNT(EG), while a less significant variation in the amount of HRP on different TNT arrays was found: 0.3 $\mu g/mm^2$ on TNT(HF), 0.52 $\mu g/mm^2$ on TNT(KF), 0.4 $\mu g/mm^2$ on TNT/N_2, and 0.24 $\mu g/mm^2$ on TNT(EG). It should be noted that TNT(EG) adsorbed the highest concentration of Th, whereas TNT(KF) adsorbed the highest amount of HRP per surface area.

3.4.2. Hydrogen Peroxide Biosensors

Figure 11 presents the CVs of TNT(HF) (plot A), TNT(KF) (plot B), TNT(EG) (plot C) and TNT/N_2 (plot D) electrodes immobilized with both HRP and Th in 0.1 M PB at pH 6.7 in the absence of H_2O_2 (dash line) and in the presence of 0.5 mM H_2O_2 (solid line) at a scan rate of 50 mV/s. The CV curves in Figure 11 show appreciably different responses of the TNT electrodes covered with Th/HRP layer. Neither reduction nor oxidation peak were observed in all four electrodes at the

Table IV. The amount of Th and HRP adsorbed on different TNT electrodes.

	Th ($\mu g/mm^2$)	HRP ($\mu g/mm^2$)	Th/HRP ratio
TNT(HF)	1.1	0.3	3.7
TNT(KF)	2.7	0.5	5.2
TNT(EG)	3.8	0.2	15.8
TNT/N_2	2.6	0.4	6.5

RESEARCH ARTICLE

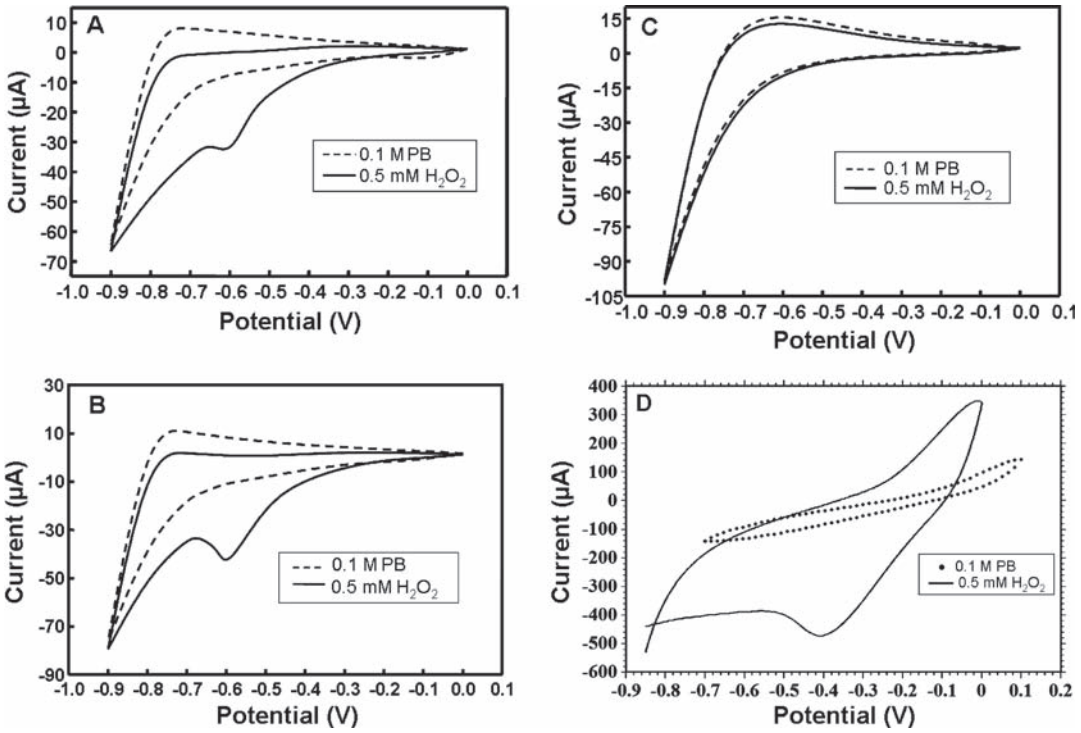

Fig. 11. Cyclic voltammograms of (A) TNT(HF) (B) TNT(KF) (C) TNT(EG) (D) TNT/N_2 in the absence (dash line) and presence (solid line) of 0.5 mM H_2O_2 at a scan rate of 50 mVs^{-1}.

absence of H_2O_2. However, a drastic increase of the reduction current of TNT(HF) (plot A) and TNT(KF) (plot B) is observed in the presence of 0.5 mM H_2O_2 (solid line). In contrast, there is no reduction peak when using TNT(EG) electrode (plot C) in the presence of 0.5 mmol H_2O_2. The difference in three TNT electrodes is likely due to the self-assembly of Th/HRP on the TNT arrays surface. Moreover, the reduction current of TNT(KF) is more negative (−47.3 μA) than TNT(HF) (−34 μA), because the TNT(KF) can adsorb more enzyme due to its larger surface area, thus the more negative increase of reduction peak for the TNT(KF) electrode shows a higher electrocatalytic activity of the immobilized HRP for Th oxidation in the presents of H_2O_2. For the TNT/N_2 electrode, the reduction current is 490 μA, 10 times larger than the current of TNT/(KF), which means a higher sensitivity to H_2O_2 than TNT(KF) and TNT(HF) electrodes, this is due to the greatly improvement of conductivity of TNT after annealed in nitrogen, this results agrees well with the EIS results. The response mechanism of the electrodes to H_2O_2 is summarized as follows:[40]

$$\text{HRP (red)} + H_2O_2 \rightarrow \text{HRP (ox)} + H_2O \quad (3)$$

$$\text{HRP (ox)} + \text{Th (red)} \rightarrow \text{HRP (red)} + \text{Th (ox)} \quad (4)$$

$$\text{Th (ox)} + 2H^+ + 2e^- \rightarrow \text{Th (red)} \quad (5)$$

Firstly the immobilized HRP (red) chemically reduces the H_2O_2 to form water and HRP (ox). Secondly the HRP (ox) chemically oxidizes the reduced Th (red) to form HRP (red) and Th (ox). Finally the Th (ox) is electrochemically reduced to form Th (red), resulting in the reduction peak at −0.6 V in the CV curves.

In addition, the reduction current increases almost linearly with an increasing concentration of H_2O_2. Although the reaction 3 is responsible to the reduction current peak, the reaction 1 is most likely the rate-limiting step. This hypothesis is supported by the fact that the reduction current peak is dependent on the concentration of H_2O_2, and the highest reduction current peak was observed in TNT(KF) with the highest amount of HRP adsorbed, followed with TNT(HF) with second highest amount of HRP, while TNT(EG) with the lowest HRP adsorbed did not show a reduction current peak at all. The above results and hypothesis would suggest to enhancing the amount of HRP adsorbed on the surface electrode for further improvements of sensing properties.

Figure 12 shows the effect of pH of the buffer solution on the performance of the TNT/N_2 electrode co-adsorbed HRP and Th at a constant concentration of 0.5 mM H_2O_2. Enzyme activity could be impacted by the pH value of buffer solution. An appropriate pH value 6.7, slightly acidic, can ensure enzyme the best activity and sensibility. When the pH value of the buffer was very low, the TNT electrode exhibited lower reduction current of H_2O_2. The highest reduction current was observed at pH of ~6.7, further increase in pH, results in a decrease in reduction peak. Although the exact mechanism to such experimental observation is not known, the following offers a possible

RESEARCH ARTICLE

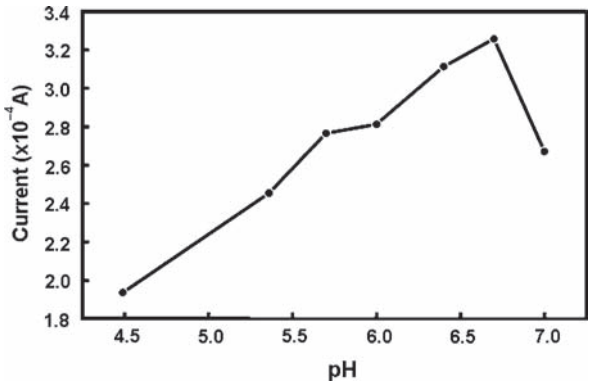

Fig. 12. Effect of pH on the response behavior of the TNT/N_2 electrode co-immobilized with thionine and HRP.

explanation. A lower pH would convert adsorbed HRP from its original state to oxidized state and, thus, hinder reaction 1 and result in a low reduction current peak. However, a high pH means low proton concentration, which in turn slows reaction 3. Obviously further experiments are needed to verify the above explanation.

Figure 13 presents the linear calibration curve of the reduction current versus the H_2O_2 concentration. The solid lines in Figure 13 are the linear fit results. The dynamic range of the sensor to the H_2O_2 concentration is from 2×10^{-5} M to 3.6×10^{-3} M for TNT/N_2 (curve a), from 1×10^{-5} M to 3×10^{-3} M for TNT(KF) (curve b) and from 5×10^{-5} M to 2×10^{-3} M for TNT(HF) (curve c). The fitting results of the three linear curves are as follow,

$$C_{TNT/N_2} = 360.87 + 89.26\ I \quad (6)$$

$$C_{TNT(KF)} = 19.61 + 21.69\ I \quad (7)$$

$$C_{TNT(HF)} = 18.27 + 14.86\ I \quad (8)$$

Where C is the concentration of H_2O_2; I refers to the reduction current. The correlation coefficients are 0.998, 0.994 and 0.992, respectively. The sensitivity to the change in the concentration of H_2O_2 as the slop of the calibration curves was 89 μA/mM for TNT/N_2, 4 times better than the sensitivity of TNT(KF) at 21 μA/mM and 6 times better than the sensitivity of TNT(HF) at 14 μA/mM. The estimated detection limits towards H_2O_2 were 0.5×10^{-5} M for TNT/N_2, and 1.2×10^{-5} M for TNT(KF) and TNT(HF). When the electrodes were not in use, they were stored in 0.1 mol PB solution in a refrigerator at 4 °C. They retained 80% of its initial current response after 1 month of storage, showing a good shelf life.

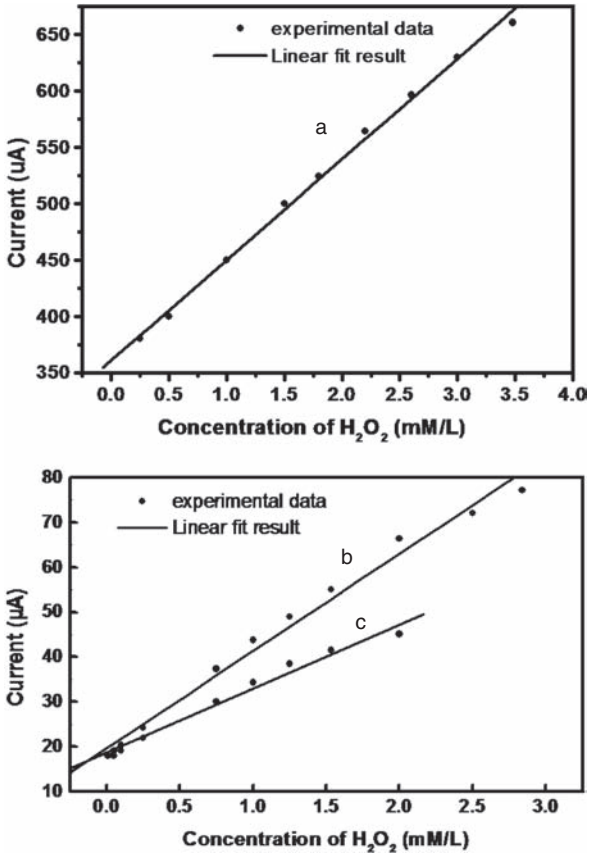

Fig. 13. Calibration curve of reduction current of TNT/N_2 (curve a), TNT(KF) (curve b) and TNT(HF) (curve c) versus the H_2O_2 concentration.

4. CONCLUSIONS

In this study, we demonstrated the electrochemical properties and biosensitivity of TiO_2 nanotubes fabricated by anodic oxidation. The results of cyclic voltammetric and EIS measurements showed that the electrical conductivity of TNT arrays was related to both of their length and calcination gas. TNT arrays annealed in nitrogen at 500 °C for 3 hrs has a 5–14 enhancement for conductivity compared with as-grown TNT and TNT annealed in air and argon. The investigation of TNT biosensor for H_2O_2 presented that the sensitivity of TNT electrode annealed in nitrogen was 4–6 times higher than the sensitivity of as-grown TNT electrodes. This allows us to develop a novel H_2O_2 sensor with a detection range from 2×10^{-5} M to 3.6×10^{-3} M. The reduction of part of Ti^{4+} and formation of oxygen vacancies in anatase titania are ascribed to explain the significantly improved electrical properties.

In summary, although only a few years have passed since their discovery, the sensing properties of the described highly ordered TNT arrays are nothing short of remarkable. As such, we believe the material architecture warrants extended and in-depth study, comparable to the efforts that have been spent investigating the properties of carbon nanotubes. Certainly, the work has only just begun in exploring the science and engineering applications of this remarkable material platform.

Acknowledgments: Peng Xiao gratefully acknowledges the fellowship from the Chinese Scholarship

RESEARCH ARTICLE

Council and the supporting of Science Foundation of Chongqing Science and Technology Committee (CSTS, 2007BB4157). This work is supported in part by National Science Foundation (DMI-0455994) and Air Force Office of Scientific Research (AFOSR-MURI, FA9550-06-1-032).

References and Notes

1. S. Iijima, *Nature* 56, 354 **(1991)**.
2. D. V. Bavykin, J. M. Friedrich, and F. C. Walsh, *Adv. Mater.* 18, 2807 **(2006)**.
3. M. Adachi, Y. Murata, M. Harada, and Y. Yoshikawa, *Chem. Lett.* 29, 942 **(2000)**.
4. S. Z. Chu, S. Inoue, K. Wada, D. Li, H. Haneda, and S. Awatsu, *J. Phys. Chem. B* 107, 6586 **(2003)**.
5. S. Uchida, R. Chiba, M. Tomiha, N. Masaki, and M. Shirai, *Electrochemistry* 70, 418 **(2002)**.
6. M. Adachi, Y. Murata, I. Okada, and Y. Yoshikawa, *J. Electrochem. Soc.* 150, G488 **(2003)**.
7. G. K. Mor, K. Shankar, M. Paulose, O. K. Varghese, and C. A. Grimes, *Nano Lett.* 6, 215 **(2006)**.
8. O. K. Varghese, D. Gong, M. Paulose, K. G. Ong, E. C. Dickey, and C. A. Grimes, *Adv. Mater.* 15, 624 **(2003)**.
9. S. Oh, R. R. Finōnes, C. Daraio, L. Chen, and S. Jin, *Biomaterials* 26, 4938 **(2005)**.
10. H. Tsuchiya, J. M. Macak, L. Müller, J. Kunze, F. Müller, P. Greil, S. Virtanen, and P. Schmuki, *J. Biomed. Mat. Res.* 77A, 534 **(2006)**.
11. J. M. Macak, H. Tsuchiya, L. Taveira, A. Ghicov, and P. Schmuki, *J. Biomed. Mat. Res.* 75A, 928 **(2005)**.
12. D. V. Bavykin, E. V. Milson, F. Marken, D. H. Kim, D. H. Marsh, D. J. Riley, F. C. Walsh, K. H. El-Abiary, and A. A. Lapin, *Electrochem. Commu.* 7, 1050 **(2005)**.
13. P. Xiao, B. B. Garcia, Q. Guo, D. W. Liu, and G. Z. Cao, *Electrochem. Commu.* 9, 2441 **(2007)**.
14. E. Topoglidis, B. M. Discher, C. C. Moser, P. L. Dutton, and J. R. Durrant, *Chem. Bio. Chem.* 4, 1332 **(2003)**.
15. K. J. McKenzie, F. Marken, and M. Opallo, *Bioelectrochemistry* 66, 41 **(2005)**.
16. M. S. Sander, M. J. Côté, W. Gu, B. M. Kile, and C. P. Tripp, *Adv. Mater.* 16, 2052 **(2004)**.
17. A. Michailowski, D. AlMawlawi, G. S. Cheng, and M. Moskovits, *Chem. Phys. Lett.* 349, 1 **(2001)**.
18. Q. Chem, W. Z. Zhou, G. H. Du, and L. H. Peng, *Adv. Mater.* 14, 1208 **(2002)**.
19. J. M. Macák, H. Tsuchiya, and P. Schmuki, *Angew. Chem. Int. Ed.* 44, 2100 **(2005)**.
20. E. Topoglidis, C. J. Camplell, A. E. G. Cass, and J. R. Durrant, *Langmuir* 17, 7899 **(2001)**.
21. S. Liu and A. Chen, *Langmuir* 21, 8409 **(2005)**.
22. G. K. Mor, O. K. Varghese, M. Paulose, K. Shankar, and C. A. Grimes, *Sol. Energy Mater. Sol. Cells* 90, 2011 **(2006)**.
23. K. Noworyta and J. Augustynski, *Electrochem. Solid State Lett.* 7, E31 **(2004)**.
24. T. Ma, M. Akiyama, E. Abe, and I. Imai, *Nano lett.* 5, 2543 **(2005)**.
25. Q. Cai, M. Paulose, O. K. Varghese, and C. A. Grimes, *J. Mater. Res.* 20, 230 **(2005)**.
26. M. Paulose, K. Shankar, H. E. Prakasam, O. K. Varghese, G. K. Mor, T. A. Latempa, A. Fitzgerald, and C. A. Grimes, *J. Phys. Chem. B* 110, 16179 **(2006)**.
27. C. Ruan, R. Yang, X. Chen, and J. Deng, *J. Electroanal. Chem.* 455, 121 **(1998)**.
28. D. Gong, C. A. Grimes, O. K. Varghese, W. C. Hu, R. S. Singh, Z. Chen, and E. C. Dickey, *J. Mater. Res.* 16, 3331 **(2001)**.
29. G. Z. Cao, Nanostructures & Nanomaterials, Imperial College Press, London **(2004)**.
30. J. S. Reed, Principles of Ceramics Processing, 2nd edn., Wiley, New York **(1995)**.
31. O. K. Varghese, D. Gong, M. Paulose, C. A. Grimes, and E. C. Dickey, *J. Mater. Res.* 18, 156 **(2003)**.
32. R. Beranek, H. Tsuchiya, T. Sugishima, J. M. Macak, L. Taveira, S. Fujimoto, H. Kisch, and P. Schmukic, *Appl. Phys. Lett.* 87, 243114 **(2005)**.
33. A. Chen and S. Nigro, *J. Phys. Chem. B* 107, 13341 **(2003)**.
34. S. Carrara, V. Bavastrello, D. Ricci, E. Stura, and C. Nicolini, *Sens. Actuators, B* 109, 221 **(2005)**.
35. M. Wang, L. Wang, G. Wang, X. Ji, Y. Bai, T. Li, S. Gong, and J. H. Li, *Biosens. Bioelectron.* 19, 575 **(2004)**.
36. E. Topoglidis, A. E. G. Cass, B.O'Regan, and J. R. Durrant, *J. Electroanal. Chem.* 517, 20 **(2001)**.
37. A. Ghicov, H. Tsuchiya, R. Hahn, J. M. Macak, A. G. Muñoz, and P. Schmuki, *Electrochem. Commun.* 8, 528 **(2006)**.
38. V. Vaithianathan, S. Hishita, J. H. Moon, and S. S. Kim, *Thin Solid Films* 515, 6927 **(2007)**.

Received: 5 February 2008. Accepted: 10 July 2008.

RESEARCH ARTICLE